

Universal 3D Shape Matching via Coarse-to-Fine Language Guidance

Qinfeng Xiao¹ Guofeng Mei² Bo Yang¹ Zhang Liying¹ Jian Zhang³ YICK Kit-lun^{1*}

¹Hong Kong Polytechnic University, HK SAR

²Fondazione Bruno Kessler, Italy

³University of Technology Sydney, Australia

qin-feng.xiao@connect.polyu.hk, kit-lun.yick@polyu.edu.hk

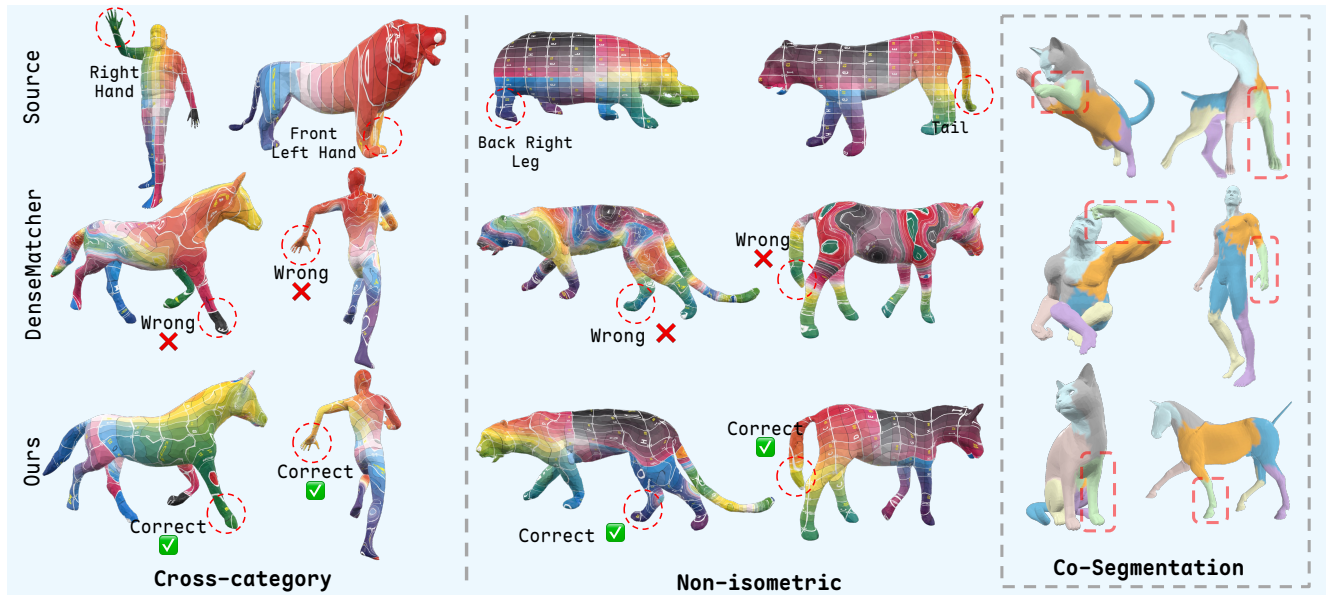


Figure 1. We propose UniMatch, a semantic-aware, coarse-to-fine framework for 3D shape matching. Our method yields high-quality semantic correspondences under challenging scenarios, *e.g.*, cross-category shapes and non-isometric deformations. Besides, UniMatch learns semantically consistent cross-shape features, enabling efficient co-segmentation for distinct categories.

Abstract

Establishing dense correspondences between shapes is a crucial task in computer vision and graphics, while prior approaches depend on near-isometric assumptions and homogeneous subject types (*i.e.*, only operate for human shapes). However, building semantic correspondences for cross-category objects remains challenging and has received relatively little attention. To achieve this, we propose **UniMatch**, a semantic-aware, coarse-to-fine framework for constructing dense semantic correspondences between strongly non-isometric shapes without restricting object categories. The key insight is to lift “coarse” semantic cues into “fine” correspondence, which is achieved

through two stages. In the “coarse” stage, we perform class-agnostic 3D segmentation to obtain non-overlapping semantic parts and prompt multimodal large language models (MLLMs) to identify part names. Then, we employ pretrained vision language models (VLMs) to extract text embeddings, enabling the construction of matched semantic parts. In the “fine” stage, we leverage these coarse correspondences to guide the learning of dense correspondences through a dedicated rank-based contrastive scheme. Thanks to class-agnostic segmentation, language guiding, and rank-based contrastive learning, our method is versatile for universal object categories and requires no predefined part proposals, enabling universal matching for inter-class and non-isometric shapes. Extensive experiments demonstrate UniMatch consistently outperforms competing

*Corresponding author

methods in various challenging scenarios.

1. Introduction

Shape matching aims to establish dense correspondences between 3D shapes and underpins a wide range of applications, such as texture transfer [18], parametric human modeling [37], robotic manipulation [63], and shape interpolation [10, 17]. A long-standing and effective paradigm represents point-to-point maps in a compact spectral representation through functional maps [46], enabling elegant regularization and efficient optimization. Deep functional map approaches further process geometric descriptors and operators in an end-to-end fashion [9, 13, 28, 31, 54]. Despite strong performance, they typically rely on a near-isometric assumption, and thus degrade under substantial non-isometric deformations or topological noises [15, 26, 46]. Moreover, purely geometric cues struggle to support inter-class matching, where correspondences between inter-class variations must bridge semantic relations [14, 63].

In parallel, visual foundation models (VFMs) have unlocked rich, transferable semantics, and surprisingly robust correspondence cues from 2D images [45, 55]. Building on these priors, recent methods lift or distill 2D features into 3D for shape matching: Diff3F [14] decorates untextured meshes with diffusion models and learn correspondences via intermediate diffusion features; DenseMatcher [63] learns 3D semantic correspondences through SD-DINO features [61] and manual annotated parts for robot manipulation; and a zero-shot pipeline, ZSC, estimates dense correspondences by feeding coarse part-level correspondences into a spectral-based refinement algorithm [1]. Although compelling, these methods remain limited: they are not versatile for in-the-wild objects in fully unsupervised settings, while ZSC requires predefined part proposals, and DenseMatcher requires manual part annotations.

To address the limitations, we propose **UniMatch**, a semantically aware, coarse-to-fine framework for computing semantic correspondences without restricting object categories. UniMatch operates in two stages. At the “coarse” stage, we first employ an effective class-agnostic 3D part segmentation algorithm to obtain non-overlapping semantic parts without predefined part proposals or category hints. Then we employ the multimodal reasoning capabilities of GPT-5 [44] to identify the name of each part and build coarse part-level correspondence by computing language embeddings using FG-CLIP [57]. At the “fine” stage, we extend the functional map framework by leveraging semantic feature fields calculated using SD-DINO [61] and the coarse correspondences. Specifically, we propose a novel group-wise rank-based contrastive loss that effectively enforces semantic consistency across shapes without requiring explicit positive/negative hints, unlike conventional con-

trastive losses. A comparison with major baselines on key features of our proposed method is summarized in Tab. 1.

Our contributions are as follows:

- We present **UniMatch**, a semantic-aware, *coarse-to-fine* shape matching framework for universal object categories without predefined part priors.
- We build coarse part-level correspondences via class-agnostic 3D part segmentation, MLLM prompting, and FG-CLIP language embeddings.
- We compute point-to-point correspondences by extending the conventional functional map framework with *semantic feature fields* and our proposed *group-wise rank-based contrastive loss* that enforces semantic consistency without explicit positives/negatives.
- Extensive experiments show consistent gains of our method on various challenging scenarios, including inter-/non-/near-isometric settings.

Table 1. Overview of our method and competing methods.

| Method | Semantic Features | Language Guided | Inter-class |
|-------------------------------|-------------------|-----------------|-------------|
| URSSM [9] [ToG 2023] | No ✗ | No ✗ | No ✗ |
| Diff3F [14] [CVPR 2024] | Yes ✓ | No ✗ | Worse |
| ZSC [1] [SIGGR. Asia 2023] | No ✗ | No ✗ | Yes ✓ |
| DenseMatcher [63] [ICLR 2025] | Yes ✓ | No ✗ | Yes ✓ |
| UniMatch (ours) | Yes ✓ | Yes ✓ | Yes ✓ |

2. Related Work

2.1. Shape Correspondences

Establishing 3D shape correspondences is crucial for various applications, and most methods can be categorized into two dominant paradigms: the functional map approach and its variants, and recent advances that leverage large-scale models to explore semantic and part-guided correspondences. Functional map [46] methods model correspondences as compact linear operators in spectral domains, applying geometric constraints for regularization. Recent advances use learned descriptors and dedicated objectives to improve matching accuracy [9, 13, 21, 28, 31, 43, 52, 54]. Though effective for near-isometric deformations, they depend on mesh assumptions and weakly capture high-level semantic structure, resulting in degraded performance under strong non-isometric or cross-category variations.

Semantic correspondences. Due to the inefficiency of conventional approaches for tackling non-isometric deformations, recent works have explored alternative approaches to find *semantic correspondences* between shapes, which are expected to capture high-level semantic relations beyond handcrafted geometric descriptors. Meanwhile, diffusion models [51] and VFMs have demonstrated strong capabilities in encoding semantic-rich features, enabling the computation of semantic correspondences across shapes. Since

these models are designed for 2D images, existing methods leverage multi-view rendering and aggregation to obtain 3D semantic features. Diff3F [14] utilizes a pre-trained diffusion model and DINO [45] to extract multi-view features, which are then aggregated to form 3D features for correspondence estimation. DenseMatcher [63] employs SD-DINO [61] features extracted from rendered images and learns matching with the help of manual part annotations.

Part-guided correspondences. 3D part segmentation can be categorized into two main approaches: text-prompted segmentation and class-agnostic segmentation. Text-prompted part segmentation lift 2D visual detectors, *e.g.* BLIP [27], from multi-view renderings and fuse the segmentation results [2, 24, 33, 62]. Instead of identifying certain parts using text prompts, class-agnostic methods decompose the entire object into semantic parts by distilling SAM masks [12, 22, 34, 58] or training in an end-to-end fashion [39, 64]. To achieve zero-shot and inter-class shape matching, ZSC [1] proposes using part segmentation to build part-level relations and refine them to produce dense correspondences. However, it relies on predefined part proposals and text prompts for each category, limiting its generalization to in-the-wild objects. DenseMatcher [63] proposes to use a contrastive loss to enforce consistency between annotated parts. Although it incorporates visual features and semantic consistency, it requires manually labeled semantic parts, which limits its broader applications in open-world scenarios.

2.2. Large-Scale Models

Recent advances in large-scale models have significantly pushed the boundaries of multimodal understanding [30, 59]. Multimodal Large Language Models (MLLMs) such as GPT-4 [3], GPT-5 [44], LLaVA [32], and QWen-VL [6] have demonstrated remarkable abilities in comprehending and reasoning about visual data in a conversational context. Concurrently, Vision-Language Models (VLMs) like CLIP [47] and its fine-grained variant FG-CLIP [57], as well as SigLIP [56], have excelled at learning powerful, generalizable visual representations from vast amounts of image-text data. These models provide robust semantic features that can be transferred to various downstream tasks. We employ the powerful multimodal reasoning capabilities of GPT-5 to identify semantic part names and leverage FG-CLIP to extract fine-grained language embeddings for building coarse part-level correspondences.

3. Method

Our method, as illustrated in Fig. 2, is a two-stage framework that operates in a coarse-to-fine manner. In the first, *coarse* stage, we prompt MLLMs to retrieve semantic regions. We then utilize language embeddings to establish semantic-rich coarse correspondences between shape pairs.

In the second, *fine* stage, these coarse correspondences “supervise” a functional map framework. This process is optimized using a dedicated group-wise ranking-based contrastive loss to yield the final dense correspondences.

3.1. The “coarse” stage: semantic region relations

Class-agnostic part segmentation. Many works utilize SAM [25] to achieve text-prompted 3D part segmentation [1, 2, 33, 40], *i.e.* using 2D visual grounding models and SAM to obtain 2D masks and aggregate them into 3D masks. In this paper, we consider an effective class-agnostic 3D segmentation method, PartField [34], instead of text-prompted segmentation. We obtain the corresponding non-intersecting 3D masks for each, representing a semantic region for the input shape \mathcal{X} . The reasons are threefold: (i) *the segmentation accuracy of text-referred methods can be disastrous for existing shape matching benchmarks, as they are often untextured and low resolution;* (ii) *text-prompted methods require explicit names of semantic parts, which are limited for open-vocabulary objects;* (iii) *even given part definitions, they cannot cover the whole shape, leading to incomplete matches for the downstream shape-matching task;* (iv) *PartField demonstrates on-the-fly inference speed due to the feedforward 3D architecture, while text-prompted 3D segmentation algorithms require complex rendering, grounding and aggregation processes.* Given an input shape \mathcal{X} and the number of parts $n_{\mathcal{R}}$, we denote the segmentation result as \mathcal{R}_x .

Multi-modal semantic region prompting. Despite the efficiency and high accuracy of class-agnostic segmentation of PartField, the semantic regions obtained have no corresponding part names. To tackle this, we prompt MLLMs to obtain a part name for each semantic region, thereby establishing coarse correspondences from the input shape pair. In detail, we first render the input shape with 3D masks into multi-view images and corresponding 2D masks using a differentiable renderer, by sequencing the cameras counterclockwise around the shape. Then, we overlay each 2D mask on the original image and prompt GPT-5 [44] to obtain the name of the shaded region. We discard too small masks, *i.e.*, less than 5% pixels out of the whole object. Finally, we aggregate part names into the 3D domain using known camera parameters to obtain the final semantic region proposal \mathcal{R}_x . More details can be found in Sec. 6.1. Compared to obtaining semantic regions with class-dependent part proposals [1], our method is more flexible in handling open-world 3D shapes and requires no predefined part proposals. Additionally, ZSC requires prompt MLLM during inference time for testing shapes. In contrast, our method only prompts MLLM for training.

Solving ambiguity by language. We attempt to build coarse correspondences among semantic regions. However, building explicit correspondences like ZSC [1] is challeng-

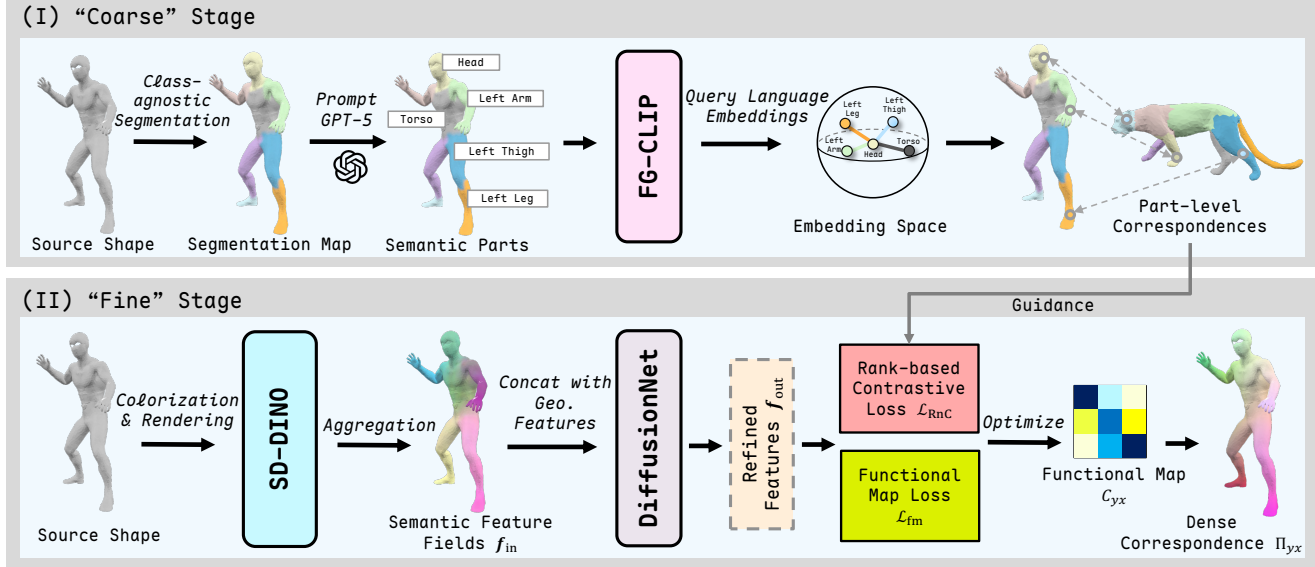


Figure 2. Our framework consists of two stages: (i) **Coarse stage**: class-agnostic 3D segmentation (PartField) produces non-overlapping semantic regions. Multi-view rendering and multimodal large language model (MLLM) prompting (using GPT-5 and FG-CLIP) assign part names and map them to unified language embeddings, enabling implicit, robust coarse correspondences across shapes. (ii) **Fine stage**: the coarse semantic matches guide dense correspondence learning within an extended functional map pipeline, leveraging SD-DINO semantic feature fields and a novel group-wise rank-based contrastive loss to enforce semantic consistency. UniMatch operates without predefined part priors and generalizes across object categories and non-isometric deformations.

ing and lacks flexibility because the input shape pair may not share the same semantic partitions, especially for cross-category shape matching. Besides, part names produced by MLLMs can be ambiguous, *e.g.* “mouth” of a human and “muzzle” of a dog should be semantically matched while they have totally different language outputs. To keep semantic consistency and robustness towards MLLM’s outputs, we build implicit correspondences between semantic regions with language embeddings. In detail, we map part names into a unified embedding space by feeding them into FG-CLIP [57] to obtain language embeddings $\mathcal{E} \in \mathbb{R}^{C_{\text{lang}}}$ where C_{lang} is the embedding dimension. Later, the similarity between the two parts can be measured using a common distance measurement. Compared with ZSC, which requires heavy MLLM prompting during inference to obtain part relations, our method only prompts GPT-5 for training data curation. We show that smooth, continuous language embeddings benefit the optimization process rather than explicit and hard-coded correspondences and reveal the semantic-rich ranks among parts in Sec. 3.2.

3.2. Fine Stage

Functional map pipeline. The functional map [46] pipeline models 3D shape correspondences as linear operators between functional spaces, typically using a spectral basis. Instead of point-to-point mapping, it computes a compact representation that can be converted back when needed [43]. We adopt the advanced variant of the func-

tional map framework, URSSM [9], in this work. Specifically, given precomputed per-vertex features \mathbf{f}_{in} for n vertices, a trainable refiner, *e.g.*, DiffusionNet [53], \mathcal{F} produces refined features: $\mathbf{f}_{\text{out}} = \mathcal{F}_{\theta}(\mathbf{f}_{\text{in}})$, where $\mathcal{F}_{\theta}(\cdot) : \mathbb{R}^{n \times C_{\text{in}}} \rightarrow \mathbb{R}^{n \times C_{\text{out}}}$. The refiner \mathcal{F} and the functional map C_{yx} are jointly optimized with: (1) data preserving loss $\mathcal{L}_{\text{data}}$ to preserve input features \mathbf{f}_{out} ; (2) regularization loss \mathcal{L}_{reg} to ensure mathematical properties like bijectivity and orthogonality; (3) coupling loss $\mathcal{L}_{\text{couple}}$ to ensure the consistency between soft correspondences (calculated by the cosine similarity of \mathbf{f}_{out}) and the functional map C_{yx} . The final functional map objective is:

$$\mathcal{L}_{\text{fm}} = \mathcal{L}_{\text{data}} + \lambda_{\text{reg}} \cdot \mathcal{L}_{\text{reg}} + \lambda_{\text{couple}} \cdot \mathcal{L}_{\text{couple}}. \quad (1)$$

This pipeline, while effective for near-isometric shapes, fails in non-isometric shape matching and heterogeneous subjects [1, 46, 63]. To this end, we enhance it by incorporating *semantic feature fields* and a *group-wise rank-based contrastive loss* for robust matching across categories and non-isometric deformations.

Semantic feature fields. Previous functional map methods [9, 21, 52] typically utilize geometric descriptors, *e.g.* wave kernel signature (WKS) [5] to feed the refiner \mathcal{F} . Inspired by the success of VFMs [11, 45, 47, 51], recent work attempts to lift 2D semantic knowledge to 3D [1, 14, 63]. Similar to DenseMatcher [63], we build our semantic fea-

ture fields using SD-DINO [61] but discard the use of positional encoding, since it results in disastrous performance. Besides, we perform view-consistent texture synthesis for uncolored shapes using SyncMVD [36], unlike textured meshes used in DenseMatcher. Then we render K multi-view RGB images with uniformly distributed elevation and azimuthal angles in $[0^\circ, 360^\circ)$. To extract semantic features, we use SD-DINO to get low-resolution features and employ the FeatUp upscaler [19] to upsample them. Lastly, given known camera parameters, we back-project and aggregate 2D semantic features into the 3D domain from all visible views. Finally, we input concatenation of the geometric descriptors \mathbf{f}_{geo} and semantic features \mathbf{f}_{sem} to the refiner \mathcal{F} :

$$\mathbf{f}_{\text{in}} = \text{Concat}(\mathbf{f}_{\text{geo}}, \mathbf{f}_{\text{sem}}). \quad (2)$$

Rank-based contrastive loss. We design a rank-based contrastive loss for learning semantic-aware correspondences. Given the shape pair \mathcal{X} and \mathcal{Y} with per-vertex features \mathbf{f}_x and \mathbf{f}_y , we use the implicit coarse correspondences to “supervise” the optimization for dense correspondences. The most straightforward solution is to adopt contrastive learning, *e.g.*, SupCon loss [23], widely used in representation learning. However, conventional contrastive losses require explicit hints to distinguish positive and negative samples, which are not available in our case. Besides, this scheme fails to recognize the underlying continuous relations between semantic regions provided by language embeddings. To tackle this, we utilize Rank-n-Contrastive (RnC) loss [60] to learn continuous representations that ordered semantic relations between parts (see Fig. 3).

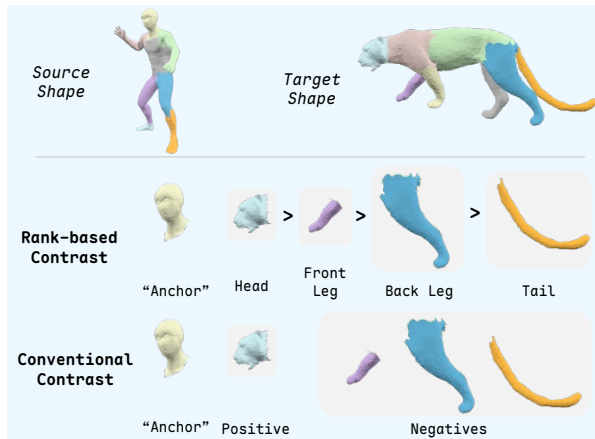


Figure 3. *Intuition of rank-based contrastive loss.* Compared with standard contrastive loss, rank-based contrastive loss effectively utilizes the ordinal hints to optimize features.

Preliminaries of RnC loss. To align the distances in the feature space ordered by similarities provided by label hints (*i.e.*, language embeddings in our case), RnC loss first ranks all samples based on label distances regarding an anchor sample, and then contrasts them according to their relative

rankings. Specifically, given an anchor \mathbf{f}_i^x , RnC loss constructs the likelihood of a reference \mathbf{f}_j^y conditioned on a set of negative samples $\mathcal{S}_{i,j} := \{\mathbf{f}_k^y | d(\mathbf{y}_i, \mathbf{y}_k) \geq d(\mathbf{y}_i, \mathbf{y}_j)\}$, which contains all samples whose ranks (defined by the label distance measure $d(\cdot, \cdot)$) to the anchor are lower than that of the reference. The likelihood is defined as:

$$\mathbb{P}(\mathbf{f}_j^y | \mathbf{f}_i^x, \mathcal{S}_{i,j}) = \frac{\exp(\text{sim}(\mathbf{f}_i^x, \mathbf{f}_j^y)/\tau)}{\sum_{\mathbf{f}_k^y \in \mathcal{S}_{i,j}} \exp(\text{sim}(\mathbf{f}_i^x, \mathbf{f}_k^y)/\tau)}, \quad (3)$$

where $\text{sim}(\cdot, \cdot)$ is the similarity measure and τ is the temperature parameter. Intuitively, maximizing $\mathbb{P}(\mathbf{f}_j^y | \mathbf{f}_i^x, \mathcal{S}_{i,j})$ increases the likelihood that samples of higher ranks than the reference \mathbf{f}_j^y and the reference are closer to the anchor \mathbf{f}_i^x than all negative samples in $\mathcal{S}_{i,j}$.

The proposed group-wise RnC loss. To supervise dense correspondences with the RnC loss, one can contrast per-vertex features using coarse semantic rankings derived from language embeddings; however, this poses $O(n_x \times n_y)$ time and memory complexity, and assumes vertex independence, ignoring the inherent grouping into semantic regions that provides structured ordinal relations. We propose a *group-wise Rank-n-Contrastive loss* that overcomes these limitations by contrasting at the semantic group level rather than per-sample, reducing complexity to $O(n_x \times n_R)$, where n_R is the number of regions ($n_R \ll n_y$), while explicitly modeling inter-group dependencies through embedding-based distances to enforce continuous semantic consistency.

Specially, given an anchor feature \mathbf{f}_i^x from the source shape and a reference group, denoted as \mathcal{G}_j^y , from the target shape, negatives $\mathcal{S}_{i,j} := \{\mathbf{f}_k^y | k \neq i, d(\mathcal{E}_i, \mathcal{E}_k) \geq d(\mathcal{E}_i, \mathcal{E}_j)\}$ are dynamically grouped by language embedding distances $d(\cdot, \cdot)$, yielding per-group likelihoods:

$$\mathbb{P}(\mathcal{G}_j^y | \mathbf{f}_i^x, \mathcal{S}_{i,j}) = \frac{\sum_l \exp(\text{sim}(\mathbf{f}_i^x, \mathbf{f}_l^y)/\tau)}{\sum_{\mathbf{f}_k^y \in \mathcal{S}_{i,j}} \exp(\text{sim}(\mathbf{f}_i^x, \mathbf{f}_k^y)/\tau)}, \quad (4)$$

where τ is the temperature parameter, and the numerator is the summation of similarities of the anchor and the reference group \mathcal{G}_j^y . The group-wise loss aggregates negative log-likelihoods over target regions:

$$\ell_{\text{RnC}}^{(i)}(\mathcal{X}, \mathcal{Y}) = \frac{1}{n_{\mathcal{R}}} \sum_{j=1}^{n_{\mathcal{R}}} -\log \mathbb{P}(\mathcal{G}_j^y | \mathbf{f}_i^x, \mathcal{S}_{i,j}). \quad (5)$$

Finally, the group-wise RnC loss is the average over source anchors, calculated by:

$$\mathcal{L}_{\text{RnC}} = \frac{1}{n_x} \sum_{i=1}^{n_x} \ell_{\text{RnC}}^{(i)}(\mathcal{X}, \mathcal{Y}). \quad (6)$$

This enables scalable, annotation-free alignment, preserves RnC’s ranking under grouped, language-guided supervision, and yields smoother, more robust correspondences than vertex-wise/independent contrasts (see Tab. 5, Fig. 4).

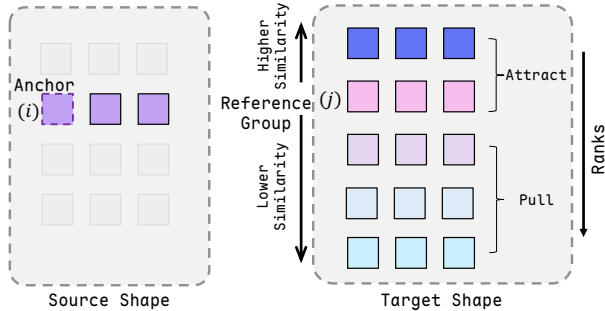


Figure 4. **Illustration of our group-wise Rank-n-Contrastive Loss.** For each **anchor** feature, we traverse the semantic regions as **reference** features, and group the negative samples by their semantic similarities (lower than reference). The darker the color, the closer the semantic similarity.

4. Experiments

4.1. Inter-class shape matching

Setup. We evaluate our method and baselines on three challenging cross-category benchmarks, Strongly Non-Isometric Shapes (SNIS) [1], TOSCA [8], and SHREC07 [20]. Details of datasets and baselines can be found in Sec. 7.1 and Sec. 8, respectively. Since no valid dense annotations are provided for inter-class matching, we follow prior works [1, 14] to compute the average geodesic error on sparse annotated vertices.

Table 2. Experimental results of inter-class shape matching. The best and the second-best are shown in **blue** and **orange** respectively.

| Method | SNIS | TOSCA | SHREC07 |
|-------------------------------|-------------|-------------|-------------|
| <i>Axiomatic Methods</i> | | | |
| ZoomOut [43] | 0.51 | 0.55 | 0.57 |
| <i>Functional Map Methods</i> | | | |
| URSSM [9] | 0.49 | 0.53 | 0.49 |
| SimpFMap [41] | 0.51 | 0.53 | 0.56 |
| <i>Semantic Methods</i> | | | |
| Diff3F [14] | 0.57 | 0.45 | 0.50 |
| ZSC [1] | 0.36 | 0.56 | 0.60 |
| DenseMatcher [63] | 0.28 | 0.30 | 0.39 |
| UniMatch (ours) | 0.19 | 0.23 | 0.37 |

Results. Tab. 2 reports the numerical results of UniMatch and representative baselines on three cross-category benchmarks. UniMatch achieves the lowest average geodesic error on all three cross-category benchmarks: 0.19 (SNIS), 0.23 (TOSCA), and 0.37 (SHREC07). This performance substantially outperforms all previous methods, including DenseMatcher, ZSC, and other functional map-based or axiomatic approaches. In detail, DenseMatcher, although competitive, falls short (0.28–0.39) compared to UniMatch, suggesting that UniMatch’s universal part seg-

mentation and group-wise contrastive loss contribute critically to more substantial semantic alignment. The visual comparison between UniMatch and DenseMatcher is shown in Fig. 5. Functional map approaches (e.g., URSSM, SimpFMap) exhibit higher errors (0.49–0.56), validating that geometric-only solutions lack sufficient flexibility for inter-class matching. This consistent margin affirms the robustness and effectiveness of the semantic-aware matching paradigm in highly challenging cross-category scenarios. The superior performance paves the way for universal, scalable matching technology for in-the-wild 3D objects.

4.2. Non-Isometric Shape Matching

Setup. We evaluate UniMatch’s performance on non-isometric shape matching using two datasets, SMAL [65] and TOPKIDS [26], which present substantial shape variations and deformations (e.g., quadruped animals and synthetic human children in different poses). We use average geodesic error ($\times 100$) as the evaluation metric. More details of datasets and baseline implementation can be found in Sec. 7.2 and Sec. 8, respectively.

Table 3. Experimental results of non-isometric shape matching.

| Method | SMAL | TOPKIDS |
|-------------------------------|------------|------------|
| <i>Axiomatic Methods</i> | | |
| ZoomOut [43] | 38.4 | 33.7 |
| Smooth Shells [16] | 36.1 | 11.8 |
| DiscreteOp [50] | 38.1 | 35.5 |
| <i>Functional Map Methods</i> | | |
| UnsupFMNet [21] | - | 38.5 |
| SURFMNet [52] | - | 48.6 |
| AttentiveFMaps [28] | 5.4 | 23.4 |
| URSSM [9] | 6.0 | 8.9 |
| <i>Semantic Methods</i> | | |
| Diff3F [14] | 28.4 | 31.0 |
| DenseMatcher [63] | 4.7 | 6.2 |
| UniMatch (ours) | 4.8 | 5.9 |

Results. Tab. 3 reports average geodesic errors ($\times 100$) on SMAL and TOPKIDS. UniMatch achieves average geodesic errors of 4.8 on SMAL and 5.9 on TOPKIDS, which is comparable or slightly better than DenseMatcher (4.7 and 6.2), and notably better than most other baselines. Functional map-based methods such as URSSM (6.0 and 8.9), AttentiveFMaps (5.4 and 23.4), and SURFMNet, as well as semantic approaches like Diff3F (28.4 and 31.0), show higher errors. The visualization results compared with the representative functional map method, URSSM, is illustrated in Fig. 6. Axiomatic methods, such as ZoomOut and Smooth Shells (38.4/33.7 and 36.1/11.8), are significantly less effective in this benchmark. The superior performance indicates that UniMatch is highly robust to substantial non-isometric deformations. The results confirm that our approach effectively overcomes limitations of prior functional

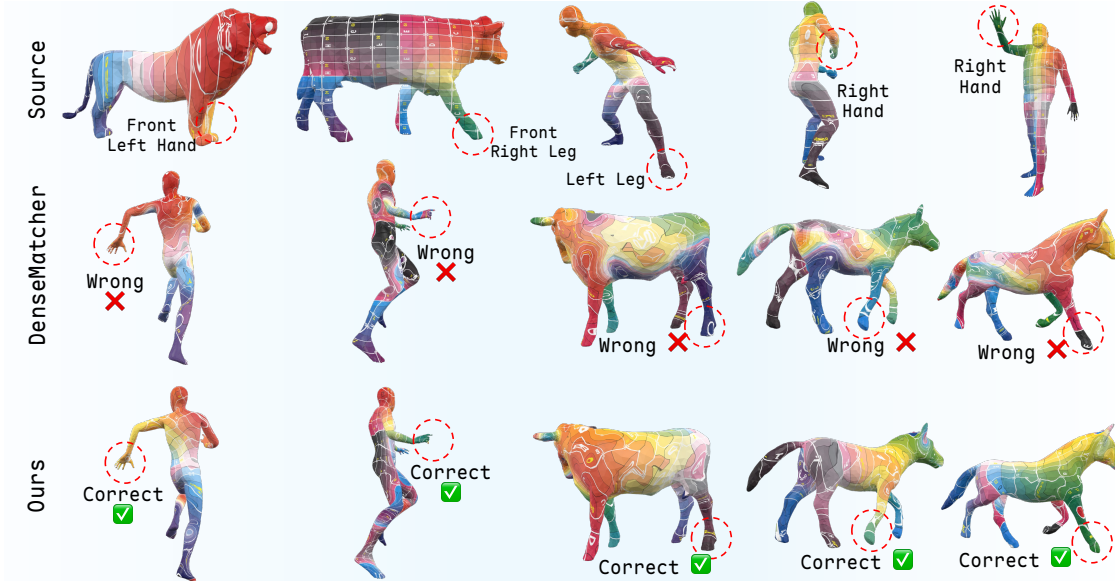


Figure 5. Visual comparison with the state-of-the-art method, DenseMatcher [63] on inter-class shape matching. UniMatch demonstrates semantic consistency and smooth correspondences for challenging cross-category matching.

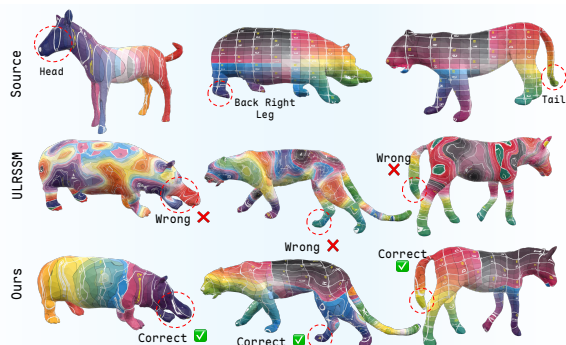


Figure 6. Visual comparison with the representative functional map method, URSSM [9] on non-isometric shapes.

map-based and semantic methods, especially for shapes that deviate strongly from near-isometric assumptions.

4.3. Near-Isometric Shape Matching

Setup. We use three widely-used benchmarks (FAUST [7], SCAPE [4], SHREC19 [42]) for near-isometric shape matching. Following [9], we consider the remeshed versions from [13] and adopt average geodesic error ($\times 100$) as the evaluation metric. Details of datasets and baselines can be found in Sec. 7.3 and Sec. 8, respectively.

Results. Tab. 4 shows the average geodesic errors achieved by our proposed method and baselines. Among all methods, UniMatch achieves state-of-the-art performance, matching or exceeding the best baseline methods on FAUST and SCAPE, and very close to the best on SHREC19. Compared to semantic-driven methods like Diff3F and DenseMatcher, UniMatch substantially reduces the geodesic error, confirming its greater accuracy. The results suggest that

Table 4. Experimental results of near-isometric shape matching.

| Method | FAUST | SCAPE | SHREC19 |
|-------------------------------|-------|-------|---------|
| <i>Axiomatic Methods</i> | | | |
| BCICP [49] | 6.4 | 11.0 | 8.0 |
| ZoomOut [43] | 6.1 | 7.5 | 7.8 |
| Smooth Shells [16] | 2.5 | 4.7 | 7.6 |
| <i>Functional Map Methods</i> | | | |
| UnsupFMNet [21] | 4.8 | 9.6 | 11.1 |
| SURFMNet [52] | 2.5 | 6.0 | 4.8 |
| URSSM [9] | 1.6 | 1.9 | 5.7 |
| <i>Semantic Methods</i> | | | |
| Diff3F [14] | 20.7 | 22.1 | 26.3 |
| DenseMatcher [63] | 1.6 | 2.0 | 3.1 |
| UniMatch (ours) | 1.6 | 1.9 | 3.2 |

UniMatch is robust to near-isometric deformations, not just cross-category or non-isometric challenges, making it universally applicable for dense shape matching tasks.

4.4. Ablation Studies

We ablate our components and design choices on SNIS, TOSCA, and SHREC07.

Language embedding calculation. We conducted an ablation study on language feature extraction to investigate the effects of different language embedding models, *e.g.* CLIP [47], SigLip [56], and the method used in this paper, FG-CLIP [57]. We design three variants that utilize language embeddings from the three models, respectively, and keep the remaining components unchanged. As shown in Tab. 5, FG-CLIP (our choice) achieves the lowest geodesic

errors (0.19/0.23/0.37), matching or slightly outperforming SigLip and clearly better than CLIP, especially on TOSCA. This demonstrates FG-CLIP’s superior capacity to deliver fine-grained, continuous semantic signals, vital for robust cross-category correspondence learning.

Semantic feature fields. To investigate the effectiveness of semantic feature fields, we ablate to evaluate the performance of the functional map with and without semantic feature fields. The first variant utilizes only geometric features, while the second variant employs both geometric and semantic features. As demonstrated in Tab. 5, removing semantic features and retaining only geometric features results in significantly higher errors (0.49/0.53/0.49), highlighting the limitation of geometric-only representations for semantic matching. Integrating semantic feature fields, as proposed, drops the errors to 0.22/0.26/0.39, confirming their critical role in bridging semantic gaps.

Rank-based contrastive loss. We also conducted an ablation study on leveraging rank-based contrastive loss to examine the effectiveness for inter-class shape matching. Compared with the variant without RnC loss, the proposed group-wise rank-based contrastive loss further enhances performance, reducing errors to 0.19, 0.23, and 0.37, indicating that harnessing the relative ordering and continuous similarity from language embeddings enables more consistent and universal correspondence alignment. We also compare our method with the SupCon loss [23], by taking the top-1 similar sample as the “pseudo” positive according to language embeddings. Employing SupCon loss yields average geodesic errors of 0.21 (SNIS), 0.29 (TOSCA), and 0.40 (SHREC07), notably higher than our group-wise RnC loss. This result reveals that SupCon loss, which relies on discrete positive selection, is less effective in capturing the continuous, semantic-rich relations between regions provided by language embeddings.

Table 5. Quantitative results of ablation study.

| | SNIS | TOSCA | SHREC07 |
|------------------------------------|-------------|-------------|-------------|
| <i>Language Embedding</i> | | | |
| CLIP | 0.21 | 0.26 | 0.37 |
| SigLip | 0.19 | 0.24 | 0.37 |
| FG-CLIP (ours) | 0.19 | 0.23 | 0.37 |
| <i>Semantic Feature Fields</i> | | | |
| w/o semantic | 0.49 | 0.53 | 0.49 |
| w. semantic (ours) | 0.22 | 0.26 | 0.39 |
| <i>Rank-based Contrastive Loss</i> | | | |
| SupCon loss | 0.21 | 0.29 | 0.40 |
| w/o contrastive loss | 0.22 | 0.26 | 0.39 |
| w. contrastive loss (ours) | 0.19 | 0.23 | 0.37 |

4.5. Co-segmentation and In-the-wild Objects

We further explore the semantic consistency of learned features through a co-segmentation task. Specifically, we first adopt agglomerative clustering to segment an anchor shape with vertex connectivity. For the target shape, we initialize K-Means clustering based on the centroids obtained from the clustering result of the anchor shape and perform the K-Means clustering on the features of the target shape. As illustrated in Fig. 7 (left), although UniMatch is not delicately designed for segmentation, our method surprisingly emerges semantic consistency across shapes with different topologies and categories. The emerging property demonstrates that UniMatch is semantic-aware.

We also conducted experiments on a broader range of objects to test the capabilities of matching for in-the-wild objects. Specifically, we evaluate our method on selected categories from SHREC07, including plane, bird, ant, octopus, chair, and table. Other categories have too fuzzy geometric characteristics, e.g., vase and mechanical part, and thus are excluded from this experiment. Despite no consistent correspondence annotations being available for these categories, we illustrate the matching results in Fig. 7 (right). UniMatch shows impressive semantic consistency across a wide range of challenging object categories, e.g., wings of a plane and a bird are correctly matched. We also investigate a failure example for the chair category, i.e., the legs are matched in the wrong order (see the purple square). The reason for such an issue is that all legs of the chair can be noted as the word “leg” and the algorithm can not infer the correct “leg” order from the given inputs. We will fix this issue by considering object orientation in future work.

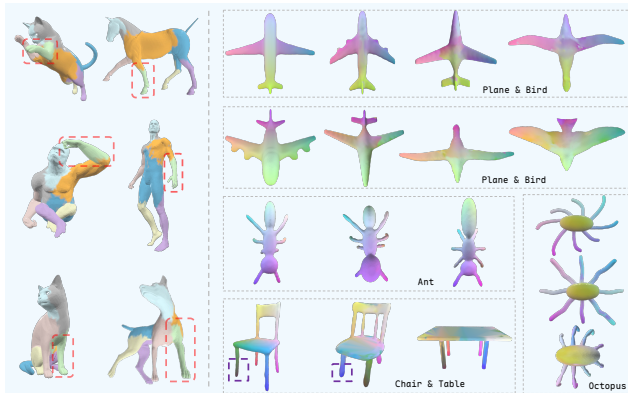


Figure 7. Left: Co-segmentation results across human and animals. Right: matching results on in-the-wild objects.

5. Conclusion

We introduce UniMatch, a semantic-aware, coarse-to-fine 3D shape matching framework that generalizes across object categories and handles strong non-isometric deformations. UniMatch employs class-agnostic part segmentation,

MLLM prompting, and fine-grained language embeddings to establish dense correspondences from coarse guidance without part priors. Experiments show UniMatch consistently outperforms existing functional map and semantic-driven methods, opening the door to universal semantic shape matching for graphics, robotics, and other domains.

References

- [1] Ahmed Abdelreheem, Abdelrahman Eldesokey, Maks Ovsjanikov, and Peter Wonka. Zero-shot 3d shape correspondence. In *SIGGRAPH Asia 2023 Conference Papers*, pages 1–11, 2023. [2](#), [3](#), [4](#), [6](#), [1](#)
- [2] Ahmed Abdelreheem, Ivan Skorokhodov, Maks Ovsjanikov, and Peter Wonka. Satr: Zero-shot semantic segmentation of 3d shapes. In *Proceedings of the IEEE/CVF International Conference on Computer Vision*, pages 15166–15179, 2023. [3](#), [1](#)
- [3] Josh Achiam, Steven Adler, Sandhini Agarwal, Lama Ahmad, Ilge Akkaya, Florencia Leoni Aleman, Diogo Almeida, Janko Altenschmidt, Sam Altman, Shyamal Anadkat, et al. Gpt-4 technical report. *arXiv preprint arXiv:2303.08774*, 2023. [3](#)
- [4] Dragomir Anguelov, Praveen Srinivasan, Daphne Koller, Sebastian Thrun, Jim Rodgers, and James Davis. Scape: shape completion and animation of people. In *ACM SIGGRAPH 2005 Papers*, pages 408–416. 2005. [7](#), [2](#)
- [5] Mathieu Aubry, Ulrich Schlickewei, and Daniel Cremers. The wave kernel signature: A quantum mechanical approach to shape analysis. In *2011 IEEE international conference on computer vision workshops (ICCV workshops)*, pages 1626–1633. IEEE, 2011. [4](#)
- [6] Jinze Bai, Shuai Bai, Yunfei Chu, Zeyu Cui, Kai Dang, Xiaodong Deng, Yang Fan, Wenbin Ge, Yu Han, Fei Huang, et al. Qwen technical report. *arXiv preprint arXiv:2309.16609*, 2023. [3](#)
- [7] Federica Bogo, Javier Romero, Matthew Loper, and Michael J Black. Faust: Dataset and evaluation for 3d mesh registration. In *Proceedings of the IEEE conference on computer vision and pattern recognition*, pages 3794–3801, 2014. [7](#), [1](#), [2](#)
- [8] Alexander M Bronstein, Michael M Bronstein, and Ron Kimmel. *Numerical geometry of non-rigid shapes*. Springer Science & Business Media, 2008. [6](#), [2](#)
- [9] Dongliang Cao, Paul Roetzer, and Florian Bernard. Unsupervised learning of robust spectral shape matching. *ACM Transactions on Graphics (TOG)*, 42(4):1–15, 2023. [2](#), [4](#), [6](#), [7](#), [1](#)
- [10] Dongliang Cao, Marvin Eisenberger, Nafie El Amrani, Daniel Cremers, and Florian Bernard. Spectral meets spatial: Harmonising 3d shape matching and interpolation. In *Proceedings of the IEEE/CVF Conference on Computer Vision and Pattern Recognition*, pages 3658–3668, 2024. [2](#)
- [11] Mathilde Caron, Hugo Touvron, Ishan Misra, Hervé Jégou, Julien Mairal, Piotr Bojanowski, and Armand Joulin. Emerging properties in self-supervised vision transformers. In *Proceedings of the IEEE/CVF international conference on computer vision*, pages 9650–9660, 2021. [4](#)
- [12] Ken Deng, Yunhan Yang, Jingxiang Sun, Xihui Liu, Yebin Liu, Ding Liang, and Yan-Pei Cao. Geosam2: Unleashing the power of sam2 for 3d part segmentation. *arXiv preprint arXiv:2508.14036*, 2025. [3](#)
- [13] Nicolas Donati, Abhishek Sharma, and Maks Ovsjanikov. Deep geometric functional maps: Robust feature learning for shape correspondence. In *Proceedings of the IEEE/CVF Conference on Computer Vision and Pattern Recognition*, pages 8592–8601, 2020. [2](#), [7](#)
- [14] Niladri Shekhar Dutt, Sanjeev Muralikrishnan, and Niloy J Mitra. Diffusion 3d features (diff3f): Decorating untextured shapes with distilled semantic features. In *Proceedings of the IEEE/CVF Conference on Computer Vision and Pattern Recognition*, pages 4494–4504, 2024. [2](#), [3](#), [4](#), [6](#), [7](#)
- [15] Roberto M Dyke, Yu-Kun Lai, Paul L Rosin, Stefano Zappalà, Seana Dykes, Daoliang Guo, Kun Li, Riccardo Marin, Simone Melzi, and Jingyu Yang. Shrec’20: Shape correspondence with non-isometric deformations. *Computers & Graphics*, 92:28–43, 2020. [2](#)
- [16] Marvin Eisenberger, Zorah Lahner, and Daniel Cremers. Smooth shells: Multi-scale shape registration with functional maps. In *Proceedings of the IEEE/CVF Conference on Computer Vision and Pattern Recognition*, pages 12265–12274, 2020. [6](#), [7](#)
- [17] Marvin Eisenberger, David Novotny, Gael Kerchenbaum, Patrick Labatut, Natalia Neverova, Daniel Cremers, and Andrea Vedaldi. Neuromorph: Unsupervised shape interpolation and correspondence in one go. In *Proceedings of the IEEE/CVF Conference on Computer Vision and Pattern Recognition*, pages 7473–7483, 2021. [2](#)
- [18] Danielle Ezuz and Mirela Ben-Chen. Deblurring and denoising of maps between shapes. In *Computer Graphics Forum*, pages 165–174. Wiley Online Library, 2017. [2](#)
- [19] Stephanie Fu, Mark Hamilton, Laura Brandt, Axel Feldman, Zhoutong Zhang, and William T Freeman. Featup: A model-agnostic framework for features at any resolution. *arXiv preprint arXiv:2403.10516*, 2024. [5](#), [1](#)
- [20] Daniela Giorgi, Silvia Biasotti, and Laura Paraboschi. Shape retrieval contest 2007: Watertight models track. 2007. [6](#), [2](#)
- [21] Oshri Halimi, Or Litany, Emanuele Rodola, Alex M Bronstein, and Ron Kimmel. Unsupervised learning of dense shape correspondence. In *Proceedings of the IEEE/CVF Conference on Computer Vision and Pattern Recognition*, pages 4370–4379, 2019. [2](#), [4](#), [6](#), [7](#)
- [22] Zhening Huang, Xiaoyang Wu, Xi Chen, Hengshuang Zhao, Lei Zhu, and Joan Lasenby. Openins3d: Snap and lookup for 3d open-vocabulary instance segmentation. In *European Conference on Computer Vision*, pages 169–185. Springer, 2024. [3](#)
- [23] Prannay Khosla, Piotr Teterwak, Chen Wang, Aaron Sarna, Yonglong Tian, Phillip Isola, Aaron Maschinot, Ce Liu, and Dilip Krishnan. Supervised contrastive learning. *Advances in neural information processing systems*, 33:18661–18673, 2020. [5](#), [8](#)

- [24] Hyunjin Kim and Minhyuk Sung. Partstad: 2d-to-3d part segmentation task adaptation. In *European Conference on Computer Vision*, pages 422–439. Springer, 2024. 3
- [25] Alexander Kirillov, Eric Mintun, Nikhila Ravi, Hanzi Mao, Chloe Rolland, Laura Gustafson, Tete Xiao, Spencer Whitehead, Alexander C Berg, Wan-Yen Lo, et al. Segment anything. In *Proceedings of the IEEE/CVF International Conference on Computer Vision*, pages 4015–4026, 2023. 3, 2
- [26] Zorah Löhner, Emanuele Rodola, Michael M Bronstein, Daniel Cremers, Oliver Burghard, Luca Cosmo, Alexander Dieckmann, Reinhard Klein, Y Sahillioğlu, et al. Shrec'16: Matching of deformable shapes with topological noise. In *Eurographics Workshop on 3D Object Retrieval, EG 3DOR*, pages 55–60. Eurographics Association, 2016. 2, 6
- [27] Junnan Li, Dongxu Li, Caiming Xiong, and Steven Hoi. Blip: Bootstrapping language-image pre-training for unified vision-language understanding and generation. In *International conference on machine learning*, pages 12888–12900. PMLR, 2022. 3
- [28] Lei Li, Nicolas Donati, and Maks Ovsjanikov. Learning multi-resolution functional maps with spectral attention for robust shape matching. *Advances in Neural Information Processing Systems*, 35:29336–29349, 2022. 2, 6
- [29] Yang Li, Hikari Takehara, Takafumi Taketomi, Bo Zheng, and Matthias Nießner. 4dcomplete: Non-rigid motion estimation beyond the observable surface. In *Proceedings of the IEEE/CVF International Conference on Computer Vision*, pages 12706–12716, 2021. 1
- [30] Zongxia Li, Xiyang Wu, Hongyang Du, Fuxiao Liu, Huy Nghiem, and Guangyao Shi. A survey of state of the art large vision language models: Alignment, benchmark, evaluations and challenges. *arXiv preprint arXiv:2501.02189*, 2025. 3
- [31] Or Litany, Tal Remez, Emanuele Rodola, Alex Bronstein, and Michael Bronstein. Deep functional maps: Structured prediction for dense shape correspondence. In *Proceedings of the IEEE international conference on computer vision*, pages 5659–5667, 2017. 2
- [32] Haotian Liu, Chunyuan Li, Qingyang Wu, and Yong Jae Lee. Visual instruction tuning. *Advances in neural information processing systems*, 36:34892–34916, 2023. 3
- [33] Minghua Liu, Yin hao Zhu, Hong Cai, Shizhong Han, Zhan Ling, Fatih Porikli, and Hao Su. Partslip: Low-shot part segmentation for 3d point clouds via pretrained image-language models. In *Proceedings of the IEEE/CVF conference on computer vision and pattern recognition*, pages 21736–21746, 2023. 3
- [34] Minghua Liu, Mikaela Angelina Uy, Donglai Xiang, Hao Su, Sanja Fidler, Nicholas Sharp, and Jun Gao. Partfield: Learning 3d feature fields for part segmentation and beyond. *arXiv preprint arXiv:2504.11451*, 2025. 3, 1
- [35] Shilong Liu, Zhaoyang Zeng, Tianhe Ren, Feng Li, Hao Zhang, Jie Yang, Qing Jiang, Chunyuan Li, Jianwei Yang, Hang Su, et al. Grounding dino: Marrying dino with grounded pre-training for open-set object detection. In *European Conference on Computer Vision*, pages 38–55. Springer, 2024. 2
- [36] Yuxin Liu, Minshan Xie, Hanyuan Liu, and Tien-Tsin Wong. Text-guided texturing by synchronized multi-view diffusion. In *SIGGRAPH Asia 2024 Conference Papers*, pages 1–11, 2024. 5, 1
- [37] Matthew Loper, Naureen Mahmood, Javier Romero, Gerard Pons-Moll, and Michael J Black. Smpl: A skinned multi-person linear model. In *Seminal Graphics Papers: Pushing the Boundaries, Volume 2*, pages 851–866. 2023. 2
- [38] Ilya Loshchilov and Frank Hutter. Decoupled weight decay regularization. *arXiv preprint arXiv:1711.05101*, 2017. 1
- [39] Changfeng Ma, Yang Li, Xinhao Yan, Jiachen Xu, Yunhan Yang, Chunshi Wang, Zibo Zhao, Yanwen Guo, Zhuo Chen, and Chunchao Guo. P3-sam: Native 3d part segmentation. *arXiv preprint arXiv:2509.06784*, 2025. 3
- [40] Ziqi Ma, Yisong Yue, and Georgia Gkioxari. Find any part in 3d. *arXiv preprint arXiv:2411.13550*, 2024. 3, 1
- [41] Robin Magnet and Maks Ovsjanikov. Memory-scalable and simplified functional map learning. In *Proceedings of the IEEE/CVF Conference on Computer Vision and Pattern Recognition*, pages 4041–4050, 2024. 6
- [42] Simone Melzi, Riccardo Marin, Emanuele Rodolà, Umberto Castellani, Jing Ren, Adrien Poulénard, et al. Shrec'19: matching humans with different connectivity. In *Eurographics Workshop on 3D Object Retrieval*. The Eurographics Association, 2019. 7, 2
- [43] Simone Melzi, Jing Ren, Emanuele Rodolà, Abhishek Sharma, Peter Wonka, Maks Ovsjanikov, et al. Zoomout: spectral upsampling for efficient shape correspondence. *ACM TRANSACTIONS ON GRAPHICS*, 38(6):1–14, 2019. 2, 4, 6, 7
- [44] OpenAI. GPT-5 System Card. Technical report, OpenAI, 2025. Accessed: 2025-08-10. 2, 3
- [45] Maxime Oquab, Timothée Darcet, Théo Moutakanni, Huy Vo, Marc Szafraniec, Vasil Khalidov, Pierre Fernandez, Daniel Haziza, Francisco Massa, Alaaeldin El-Nouby, et al. Dinov2: Learning robust visual features without supervision. *arXiv preprint arXiv:2304.07193*, 2023. 2, 3, 4
- [46] Maks Ovsjanikov, Mirela Ben-Chen, Justin Solomon, Adrian Butscher, and Leonidas Guibas. Functional maps: a flexible representation of maps between shapes. *ACM Transactions on Graphics (ToG)*, 31(4):1–11, 2012. 2, 4
- [47] Alec Radford, Jong Wook Kim, Chris Hallacy, Aditya Ramesh, Gabriel Goh, Sandhini Agarwal, Girish Sastry, Amanda Askell, Pamela Mishkin, Jack Clark, et al. Learning transferable visual models from natural language supervision. In *International conference on machine learning*, pages 8748–8763. PmlR, 2021. 3, 4, 7
- [48] Nikhila Ravi, Jeremy Reizenstein, David Novotny, Taylor Gordon, Wan-Yen Lo, Justin Johnson, and Georgia Gkioxari. Accelerating 3d deep learning with pytorch3d. *arXiv:2007.08501*, 2020. 1
- [49] Jing Ren, Adrien Poulénard, Peter Wonka, and Maks Ovsjanikov. Continuous and orientation-preserving correspondences via functional maps. *ACM Transactions on Graphics (ToG)*, 37(6):1–16, 2018. 7, 2
- [50] Jing Ren, Simone Melzi, Peter Wonka, and Maks Ovsjanikov. Discrete optimization for shape matching. In *Computer Graphics Forum*, pages 81–96. Wiley Online Library, 2021. 6

- [51] Robin Rombach, Andreas Blattmann, Dominik Lorenz, Patrick Esser, and Björn Ommer. High-resolution image synthesis with latent diffusion models. In *Proceedings of the IEEE/CVF conference on computer vision and pattern recognition*, pages 10684–10695, 2022. 2, 4
- [52] Jean-Michel Roufosse, Abhishek Sharma, and Maks Ovsjanikov. Unsupervised deep learning for structured shape matching. In *Proceedings of the IEEE/CVF International Conference on Computer Vision*, pages 1617–1627, 2019. 2, 4, 6, 7
- [53] Nicholas Sharp, Souhaib Attaiki, Keenan Crane, and Maks Ovsjanikov. Diffusionnet: Discretization agnostic learning on surfaces. *ACM Transactions on Graphics (TOG)*, 41(3): 1–16, 2022. 4, 1
- [54] Mingze Sun, Shiwei Mao, Puhua Jiang, Maks Ovsjanikov, and Ruqi Huang. Spatially and spectrally consistent deep functional maps. In *Proceedings of the IEEE/CVF International Conference on Computer Vision*, pages 14497–14507, 2023. 2
- [55] Luming Tang, Menglin Jia, Qianqian Wang, Cheng Perng Phoo, and Bharath Hariharan. Emergent correspondence from image diffusion. *Advances in Neural Information Processing Systems*, 36:1363–1389, 2023. 2
- [56] Michael Tschannen, Alexey Gritsenko, Xiao Wang, Muhammad Ferjad Naeem, Ibrahim Alabdulmohsin, Nikhil Parthasarathy, Talfan Evans, Lucas Beyer, Ye Xia, Basil Mustafa, et al. Siglip 2: Multilingual vision-language encoders with improved semantic understanding, localization, and dense features. *arXiv preprint arXiv:2502.14786*, 2025. 3, 7
- [57] Chunyu Xie, Bin Wang, Fanjing Kong, Jincheng Li, Dawei Liang, Gengshen Zhang, Dawei Leng, and Yuhui Yin. Fg-clip: Fine-grained visual and textual alignment. *arXiv preprint arXiv:2505.05071*, 2025. 2, 3, 4, 7
- [58] Yunhan Yang, Yukun Huang, Yuan-Chen Guo, Liangjun Lu, Xiaoyang Wu, Edmund Y Lam, Yan-Pei Cao, and Xihui Liu. Sampart3d: Segment any part in 3d objects. *arXiv preprint arXiv:2411.07184*, 2024. 3
- [59] Shukang Yin, Chaoyou Fu, Sirui Zhao, Ke Li, Xing Sun, Tong Xu, and Enhong Chen. A survey on multimodal large language models. *National Science Review*, 11(12): nwa403, 2024. 3
- [60] Kaiwen Zha, Peng Cao, Jeany Son, Yuzhe Yang, and Dina Katabi. Rank-n-contrast: learning continuous representations for regression. *Advances in Neural Information Processing Systems*, 36:17882–17903, 2023. 5
- [61] Junyi Zhang, Charles Herrmann, Junhwa Hur, Luisa Polania Cabrera, Varun Jampani, Deqing Sun, and Ming-Hsuan Yang. A tale of two features: Stable diffusion complements dino for zero-shot semantic correspondence. *Advances in Neural Information Processing Systems*, 36:45533–45547, 2023. 2, 3, 5
- [62] Yuchen Zhou, Jiayuan Gu, Xuanlin Li, Minghua Liu, Yunhao Fang, and Hao Su. Partslip++: Enhancing low-shot 3d part segmentation via multi-view instance segmentation and maximum likelihood estimation. *arXiv preprint arXiv:2312.03015*, 2023. 3
- [63] Junzhe Zhu, Yuanchen Ju, Junyi Zhang, Muhan Wang, Zhecheng Yuan, Kaizhe Hu, and Huazhe Xu. Densmatcher: Learning 3d semantic correspondence for category-level manipulation from a single demo. In *ICLR*, 2025. 2, 3, 4, 6, 7
- [64] Zhe Zhu, Le Wan, Rui Xu, Yiheng Zhang, Honghua Chen, Zhiyang Dou, Cheng Lin, Yuan Liu, and Mingqiang Wei. Partsam: A scalable promptable part segmentation model trained on native 3d data. *arXiv preprint arXiv:2509.21965*, 2025. 3
- [65] Silvia Zuffi, Angjoo Kanazawa, David W Jacobs, and Michael J Black. 3d menagerie: Modeling the 3d shape and pose of animals. In *Proceedings of the IEEE conference on computer vision and pattern recognition*, pages 6365–6373, 2017. 6, 1, 2

Universal 3D Shape Matching via Coarse-to-Fine Language Guidance

Supplementary Material

6. Implementation Details

6.1. Details of MLLM prompting

After class-agnostic segmentation, we first render 3D objects with 3D masks into 2D images, by a front view and a back view, as shown in Fig. 8. We discard too small masks, *i.e.*, less than 5% pixels out of the whole object. This ratio is selected empirically to avoid misleading GPT-5. Similar to Find3D [40], we later feed the images into GPT-5 and the following prompt to obtain part names:

```
Infer region names
```

```
- What is the name of the part that is masked as [COLOR]?  
If you cannot find the part visible or are not sure, just  
say unknown. Only output one word or one phrase.
```

Finally, we aggregate part names into the 3D domain using known camera parameters to obtain the final semantic region proposal. As shown in Fig. 8, although the same concept can be expressed in different ways (*e.g.*, body and torso), our method can flexibly match them.

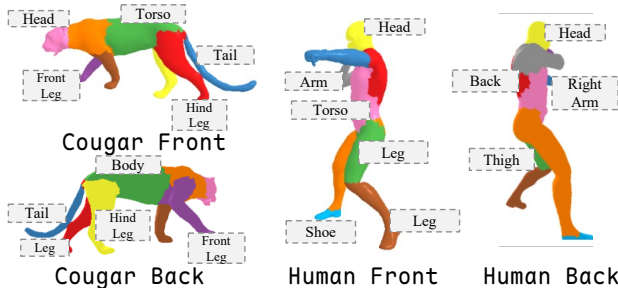


Figure 8. Examples of mask rendering and part names obtained from GPT-5.

6.2. Details of UniMatch

Class-agnostic segmentation. We consider an effective class-agnostic 3D segmentation method, PartField [34] to segment the 3D shape into non-intersecting parts. The number of semantic parts $n_{\mathcal{R}}$ is selected empirically to provide enough semantic information and avoid over-segmentation. We use $n_{\mathcal{R}} = 9$ for human data and $n_{\mathcal{R}} = 8$ for animal data. We also illustrate the segmentation results from PartField [34] and text-prompted method SATR [2] in Fig. 9. Compared with PartField, the segmentation results of SATR contain significant noise and ambiguous boundaries.

Semantic feature fields. We first perform view-consistent texture synthesis, SyncMVD [36], for uncolored



Figure 9. Comparison between class-agnostic segmentation PartField [34] and text-prompted segmentation SATR [2]. Different parts are rendered in random colors.

shapes and render them into K multi-view RGB images using PyTorch3D [48] ($K = 10$ for all experiments). We use uniformly distributed elevation and azimuthal angles in $[0^\circ, 360^\circ)$. Then we extract semantic features using SD-DINO and employ the FeatUp upscaler [19] to upsample them. Lastly, we back-project 2D semantic features into the 3D domain from all visible views using known camera parameters and average them to obtain per-vertex features.

Network and functional map. We use DiffusionNet [53] as our feature refiner \mathcal{F} . The dimensions of \mathbf{f}_{geo} and \mathbf{f}_{sem} are 128 and 768 respectively. The output dimension of \mathbf{f}_{out} is 256. For functional map calculation, we empirically set $\lambda_{\text{couple}} = 1.0$ and $\lambda_{\text{reg}} = 1.0$ in Eq. (1), following URSSM [9].

Training. We use the AdamW [38] optimizer with learning rate 10^{-3} for all experiments. We train our framework for 15 epochs.

7. Details of Datasets

7.1. Inter-Class Datasets

- **SNIS** [1] is a dataset to test strongly non-isometric and cross-category matching (*e.g.* a human vs. a dog), containing 211 shapes from different sources, including FAUST [7] (human), SMAL [65] (animals), and DeformingThings4D (DT4D) [29] (humanoid). Annotations include 34 semantically corresponding keypoints for each

shape. We use 250 test pairs provided by SNIS for evaluation (all test pairs are cross-category) and other pair combinations for training. Fig. 10 shows some example pairs from SNIS.

- **TOSCA** [8] consists of synthetic high-resolution meshes of humans and animals captured in different poses. It contains 80 objects that span several categories, including cats, dogs, horses, centaurs, gorillas, humans, *etc.* We remesh the original meshes to keep about 10,000 faces. Since no cross-category annotations are provided, we prompted GPT-5 to find semantically matched keypoints between categories and finally filtered 20 keypoints. Similar with SNIS, we randomly select half samples from each category, and build the test pairs cross categories, result in 380 pairs for evaluation. We use the rest pair combinations for training.
- **SHREC07** [20] consists of 400 watertight shapes and 20 semantic categories with 20 shapes per class, representing a wide range of objects such as humanoids, mechanical parts, animals, and furniture. Since some categories contain extremely sparse keypoints and share almost no common structures, *e.g.* table, vase, and fish, we only conduct experiments on filtered categories, including human, teddy, armadillo, and four-legged animals, and prompted GPT-5 to find semantically matched keypoints between them, finally obtaining 15 keypoints. Similar to TOSCA, we randomly select half samples from each category, and build 100 pairs for evaluation and the rest pair combinations for training.

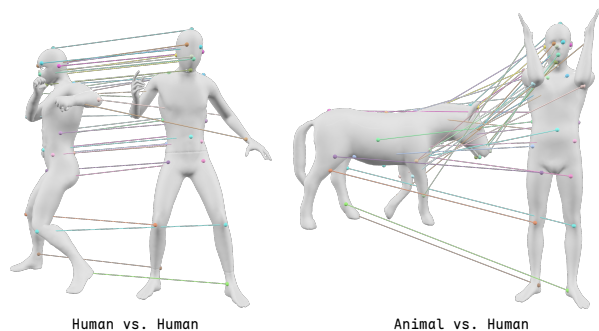


Figure 10. Example shape pairs and annotations from SNIS [1]. SNIS contains strongly non-isometric and cross-category shape pairs, such as human vs. animal and human vs. humanoid, with semantically annotated keypoint correspondences.

7.2. Non-Isometric Datasets

- **SMAL** [65] contains 49 four-legged animal shapes representing 8 species, such as dogs, cats, lions, horses, and *etc.* Each shape is represented as a watertight mesh with about 8,000 faces. Following Cao et al. [9], we use five species for training and three unseen species for evalua-

tion.

- **TOPKIDS** [26] is designed for evaluating non-isometric deformations and topological noises. It contains 26 shapes of synthetic human (“fat kid”) in various poses. Each shape includes ground-truth dense correspondences to a reference template shape.

7.3. Near-Isometric Datasets

- **FAUST** [7] consists of 10 human subjects with 10 different poses, where 80 shapes are provided for training and 20 shapes for testing. Following Cao et al. [9], we consider the remeshed versions from Donati et al. [13]. Each shape contains around 5,000 vertices with ground-truth dense correspondences to a template shape.
- **SCAPE** [4] contains 71 human shapes with various poses of the same person. The dataset is split into 51 training shapes and 20 testing shapes.
- **SHREC19** [42] is a benchmark to evaluate non-rigid shape matching, with a particular focus on different mesh connectivities in human shapes. It contains 44 human shapes with various identities and poses.

8. Details of Baselines

For URSSM [9], we use the same training scheme and parameter settings with UniMatch. *To keep a fair comparison, we disable the test-time adaptation.* For Diff3F [14], we follow the original implementation. Since the code of ZSC [1] is not open-source, we implement it according to the original paper. We use Grounding-DINO [35] for visual grounding and SAM [25] to obtain masks. Given segmentation results, the final dense correspondences are calculated by BCICP [49]. For DenseMatcher [63], we use the same training scheme, parameter settings, and the same semantic features on textured meshes with UniMatch. Since DenseMatcher requires predefined semantic parts, we use the same segmentation results of ZSC.

9. Limitation and Future Work

While UniMatch demonstrates strong performance in universal 3D shape matching under non-isometric and inter-class scenarios, several limitations remain. First, GPT-5 may fail to correctly order symmetric or repetitive parts (*e.g.*, chair legs), as semantic part names alone cannot infer geometric arrangement. Incorporating explicit object orientation cues or relational priors may alleviate such issues. Second, our method still needs a separate procedure to extract semantic features using vision foundation models. Training a unified feed-forward feature extractor that distills visual knowledge from foundation models, rather than a feature refiner, may address this issue. Finally, the current framework relies on multimodal large language models for prompting during training-time part naming to en-

able semantic awareness. Extending this to more efficient pipelines could improve scalability and practicality. Future work will address these challenges by exploring enhanced structural priors of shapes, a unified feed-forward feature extractor, and reducing model intervention during matching.